metals

MDPI

Article

Influence of Different Soaking Times at 1050 °C on the UT Response Due to Microstructure Evolution of 2205 Duplex Stainless Steel

Andrea Gruttadauria, Silvia Barella *, Carlo Mapelli and Davide Mombelli

Dipartimento di Meccanica, Politecnico di Milano, via La Masa 1, 20156 Milano, Italy; andrea.gruttadauria@polimi.it (A.G.); carlo.mapelli@polimi.it (C.M.); davide.mombelli@polimi.it (D.M.)

* Correspondence: silvia.barella@polimi.it; Tel.: +39-0223998662

Received: 16 March 2020; Accepted: 10 April 2020; Published: 11 April 2020

Abstract: Under standard conditions, DSS (duplex stainless steel) features differing amounts of ferrite and austenite, essentially depending on the thermal treatment performed. This study is focused on the ultrasonic tests (UTs) response of DSS 2205, as a function of the microstructure, in terms of austenite volume fraction and austenitic grains evolution owing to different soaking times at 1050 °C. UTs were carried out on several samples. The samples underwent varying thermal treatments characterized by a constant maintenance temperature with different soaking times that allowed for microstructure evolution and modification of the structural constituents' fraction. The UTs have highlighted an attenuation trend with the response mainly dependent upon the wave scattering and energy absorption caused by the grain features. In particular, the peak of sound attenuation was shown to correspond with the microstructure, which featured a major amount of austenite (in terms of volume fraction and the grain dimensions) and the disappearance of austenitic precipitates within the ferritic matrix. In order to obtain less UT attenuation, without affecting the mechanical and corrosion properties, the soaking should last as little time as possible.

Keywords: duplex stainless steel; ultra-sonic tests; waves attenuation; isothermal annealing

1. Introduction

During manufacturing, determining the soundness of material is crucial in ensuring the properties of the components in field. For this reason, non-destructive testing (NDT) is essential and often mandatory before and during the commissioning of components [1].

As the ultrasonic beam crosses the material, its intensity decreases owing to sound energy loss. This is caused by diffraction, scattering, and absorption mechanisms that take place within the medium [2].

The factors that are primarily responsible for the beam intensity loss are transmission losses (absorption), interference effects (diffraction), and beam scattering [3]. Moreover, the propagation of ultrasonic waves in crystalline materials is subjected to the interaction with defects (such as non-metallic inclusions, porosities, and micro-cracks) that cause sound attenuations and variation in the sound propagation velocity [4–6]. Furthermore, an ultrasonic wave traveling in such an inhomogeneous medium undergoes multiple reflection, transmission, and mode conversion (i.e., scattering) at grain boundaries and, therefore, the ultrasound beam gets attenuated. Grain scattering depends mainly on the elastic anisotropy of the grains, grains' geometric features, grain boundaries, and texture [7–9].

Duplex stainless steels have an attractive combination of mechanical and corrosion properties that make them suitable for many marine and petro-chemical applications. This study aims to affirm a relationship between ultrasonic attenuation and the lattice features of 2205 duplex stainless steel.

Duplex stainless steel (DSS) has higher strength properties than austenitic stainless steel, a superior toughness to the ferritic, good weldability, and high resistance to pitting and stress corrosion cracking. These unique properties depend on the amount and distribution of austenite and ferrite, which further depend on the maintenance temperature of the annealing treatments. It is well known that the best compromise between chemical and mechanical properties is obtained by a phase ratio equal to 50:50, reached by a solution annealing at 1050 °C followed by water quenching.

During duplex ultrasonic test (UT) investigation, it is important to consider the variation in wave propagation behaviour in the two different phases. In particular, propagation is hindered in the austenitic phase mainly because of its FCC (face-centered cubic) cell because of the strong attenuation of ultrasound. The FCC lattice is characterized by a large number of normal vibrational modes with respect to that of the ferritic matrix, which is BCC (body-centered cubic) [10]. The vibrational modes are related to the cell slip systems (a combination of slip planes and slip directions) and are higher in austenite than ferrite (at room temperature) [11]. Many slip systems imply many vibrational modes, which further implies a major vibrational capacity, which in turn causes a decrease in the propagation energy. Moreover, the cell parameters of the BCC are smaller than those of the FCC cell in terms of interatomic distance, implying a higher propagation facility [10]. However, when comparing the theories and results of several researchers, it must be concluded that the effects of crystalline architecture are not yet really clarified [8].

The grain size is another factor that must be considered as it can modify the UT response, with the attenuation increasing as the grain size increases [3]. Indeed, an increase in grain size corresponds to an increase in thermo-elastic losses (especially heat losses), causing the material's transparency conditions to worsen. In general, the larger grain has significant defects that result in wave energy dissipation. Theoretically, the attenuation of ultrasound is smaller in a single crystal than in polycrystalline materials, because the scattering at grain boundaries is missing. In polycrystalline materials, the grain boundary scattering is also larger the more anisotropic the material, that is, the more the acoustic impedances of the adjacent grains differ from each other. The velocity thus varies from grain to grain, leading to strong reflections at the grain boundaries and, therefore, to strong attenuation. The reflection and transmission phenomena at interfaces between two anisotropic materials are more complicated owing to the quasi nature of waves and beam skewing, which means that—unlike in isotropic materials—the energy flow direction generally does not coincide with the direction of wave propagation. Further, all three wave modes couple at the interface in the case of anisotropic materials [7,8].

According to [12], it is possible to have different types of scattering in relation to the difference between wavelength (λ) and grain size (D): Rayleigh scattering (λ >> D), stochastic scattering (λ~D), and diffusive scattering (λ < D). Moreover, in the case of Rayleigh scattering, it is possible to introduce the ξ, factor (E1) as follows:

$$\xi = 0.01 * \lambda = 0.01 * V/\upsilon \quad (1)$$

where λ is the wavelength, V is the sound speed in the medium, and υ is the sound frequency. This factor allows to correlate the grain size with the attenuation mechanism: if the average grain size is lower than ξ, attenuation is dominated by absorption phenomena; if the average grain size is > ξ, the scattering conditions are satisfied [3].

Another important factor to consider is the hysteresis caused by the wave propagation; the hysteresis appears when the entire wave period is present in a single grain, implying that a portion of the grain was stimulated by the wave crest and the other by the wave trough. This difference in behaviour leads to heat generation (energy loss) and wave attenuation [13].

It is also important to focus attention on the grain boundary itself. By its nature, the grain boundary is characterized by an unordered structure and the presence of discontinuities. On one hand, this leads to wave attenuation, while on the other, it implies a structure characterized by low vibrational modes, thus less capacity for motion and, consequently, attenuation. In this context, a finer grain involves substantial grain boundaries and a consequent decrease in attenuation.

In the present study, ultrasonic investigations have been employed to characterize the influence of microstructural features (in terms of austenite quantity and distribution) on sound absorption during NDT investigation in specimens characterized by different annealing soaking times. This means a slight difference in austenite amount [14].

2. Experimental Procedure

2.1. Specimens' Preparation and Heat Treatments

DSS 2205 was analysed and the chemical composition is reported in Table 1.

Table 1. Composition by quantometer (analyses performed by Spectromax X) of duplex stainless steel (DSS) 2205 grade stainless steels (in weight %).

Element	C	Mn	Si	P	S	Cr	Mo	Ni	Fe	N
wt. %	0.025	1.80	0.90	0.022	0.010	22.5	3.0	5.5	bal.	0.20

The specimens were taken from a bar (40 × 25 mm) 600 mm in length. The bar was obtained by hot forging (reduction ratio equal to 5) and it was then annealed at 1040 °C for 1 h and water quenched. This treatment provided the standard initial condition, in terms of chemical homogenization, distribution, and morphology of the phases, for the subsequent treatment. From this bar, six approximately 100 mm in length specimens were drawn. These were heated in an electric muffle furnace at the same temperature (1050 °C) for different times in order to promote a particular microstructural evolution (Table 2).

Table 2. Solution-annealing parameters applied to each coupon.

Nomenclature	Temperature [°C]	Time [hours]	Cooling
as-received	1040	1	Water cooling
F1/2	1050	0.5	Water cooling
F1	1050	1	Water cooling
F2	1050	2	Water cooling
F4	1050	4	Water cooling
F8	1050	8	Water cooling

2.2. Etching, Grain Features, and Hardness Test

Metallographic analyses by means of optical microscopy were performed on each sample after standard surface preparation and Beraha's tint etching [15]. The amounts of austenite and ferrite fractions were measured by Fisher MP30 ferritoscope. The hardness of each phase was measured using a Vicker's (HV) hardness tester at a test load of 300 g at room temperature for 15 seconds. A Brinell hardness test (HB) was performed as well using a 5 mm penetrator diameter while applying a load of 5000 g for 20 s. The hardness tests were performed according to UNI EN ISO 6507-1 (1999) and UNI EN ISO 6506-1 (2001). The chemical characterization of the different structural constituents was performed by SEM (scanning electron microscopy) equipped with an EDS (Energy Dispersive X-ray Spectrometry) probe in order to perform a localized chemical analysis.

2.3. Attenuation Measurements

Ultrasonic tests were performed according to the contact pulse-echo method by Krautkramer USN 60 unit (GE, Wunstorf, Germany) using a 2 MHz longitudinal wave probe at room temperature. The tests were performed on the major axes of the samples and the wave was propagated parallel to the metallographic section. Ultragel was used as a couplant for the probe [16].

Attenuation refers to sound energy loss, as the ultrasonic beam passes through the material, and can be determined by evaluating the multiple backwall reflections visible on a A-scan display

(amplitude mode display, represent the amount of received ultrasonic energy as a function of time). The amplitude difference between two adjacent signals is then measured and divided by the time interval. This calculation determines an attenuation coefficient in decibels per meter [17].

3. Results

The comparison of the duplex structures obtained after different soaking annealing times is reported in Figure 1.

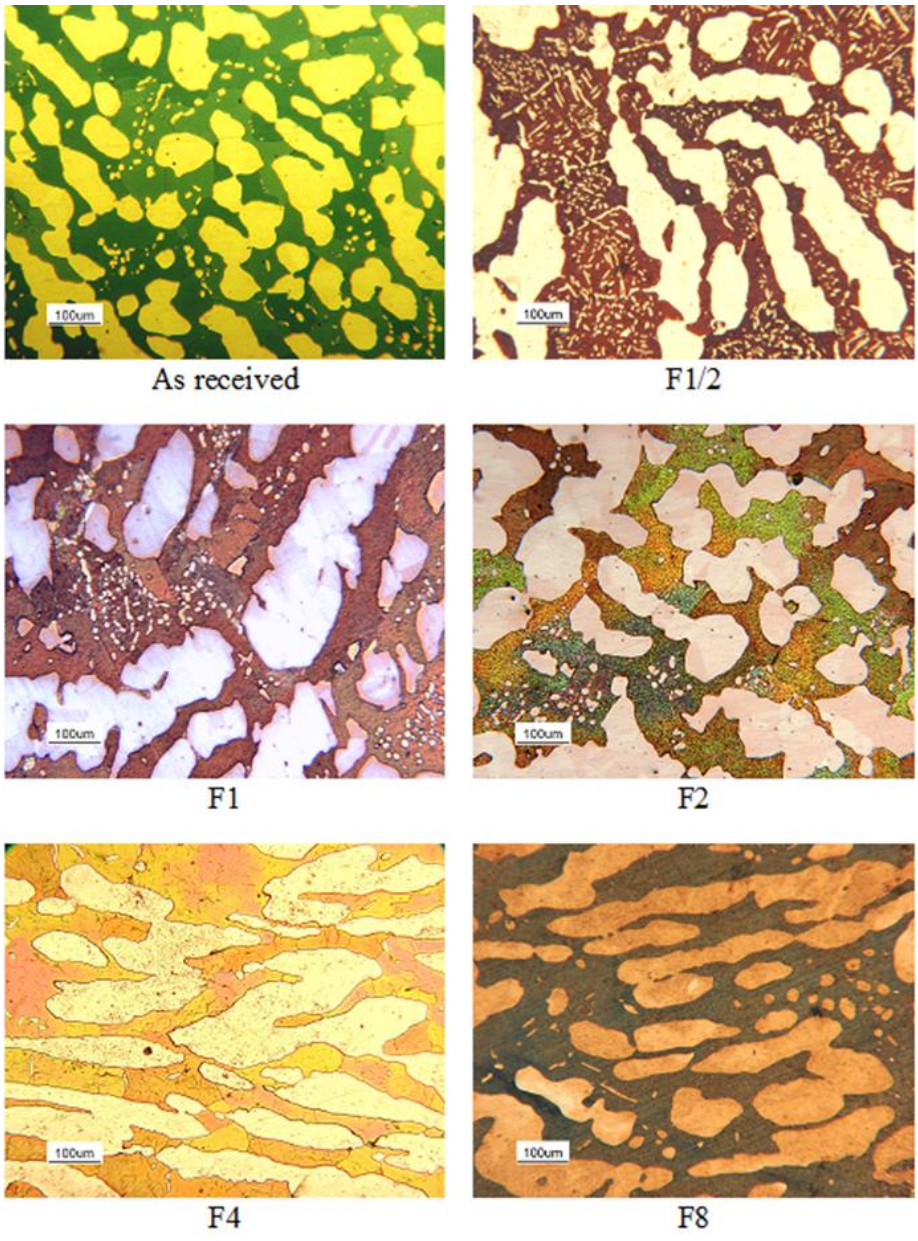

Figure 1. Microstructures of duplex stainless steel (DSS) 2205 thermal treated at 1050 °C for different soaking times.

All of the specimens are characterized by a biphasic structure, featured by a ferritic matrix and dispersion of austenitic grains in different morphologies. The difference in phase volume fractions was determined by the thermal treatment parameters. The main effect is because of the temperature, more specifically, an increase in temperature corresponds to an increase in ferrite fraction [18]. The treatment time (at a constant temperature) was also important for the kinetic microstructure because it influenced

the phase; the phases tend towards the equilibrium and it is reached not asymptotically and immediately, but by a fluctuating trend [14].

Figure 2 is useful to summarize the different morphologies of the austenite phase that can be recognized in a duplex stainless-steel microstructure: islands (I), Widmanstätten (W), and polygonal (P) and round-shape grains (R). The islands derived from the eutectoid transformation (during solidification and cooling) and from the coarsening of smaller grains during the soaking treatment. The Widmanstätten structure developed from the island, or at the ferrite–ferrite grain boundaries, during the first stage of annealing. The round-shape grains, originating from a martensitic shear process, occurred only at the end of the thermal treatment. These grains resulted from a crystallographic rotation in a polygonal shape (P in Figure 2) and then grew into the ferritic matrix, assuming their round shape because of diffusion mechanisms [11,18–20].

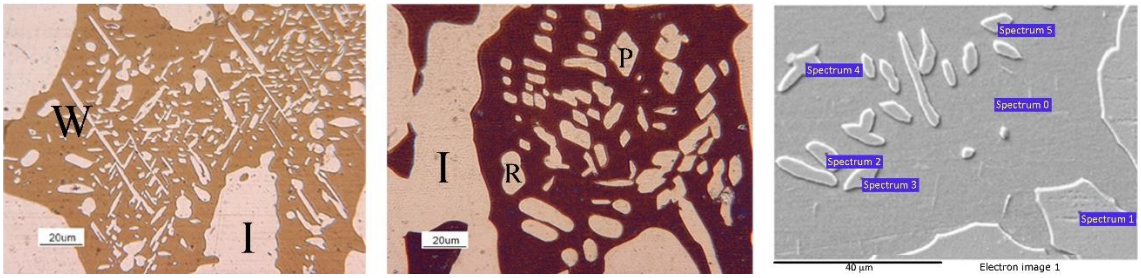

(**a**) (**b**) (**c**)

Figure 2. Microstrcture of F1/2 (**a**), F1 (**b**), and scanning electron microscopy (SEM) caption on sample F1/2 for EDS analyses (**c**). Particulars of the DSS microstructure with varying austenite shapes, it is possible to distinguish the following: austenitic islands (I), Widmanstetten arms (W), and (**b**) polygonal (P) and round-shape grains (R).

Initially, austenite precipitates at the ferrite/ferrite grain boundaries and grows through the Widmanstätten morphology into the interior of the grains. Afterwards, austenite also precipitates as intra-granular side-plate islands. The rate of this reaction is very fast and the ferrite decomposition is fulfilled in a few minutes. As the soaking times of the annealing thermal treatment increase, the fine dispersion of nuclei decreases and their larger average size witnesses the competitive character characterizing this growth stage [14].

Table 3 shows the precise chemical analysis carried out on the different phases characterizing the microstructure. It is noted that the matrix, being ferritic, is richer in α-stabilizing elements such as Cr and Mo. On the other hand, the dispersed phases in the matrix show an increase in γ-stabilizer, rich in Ni and Mn, but poor in Cr and Mo. This confirms that the dispersed phases in the matrix are actually all austenitic characterized by different morphologies (I, W, R, P) owing to the different nucleation typologies.

Sample F1/2 shows austenitic islands and a high quantity of Widmanstätten grains, characterized by an elongated shape of about 19 µm in length and 4 µm in width. Besides the Widmanstätten growth, a martensitic shear process has taken place (at the ferrite–ferrite grain boundaries) and this process was responsible for the presence of the round-shape grains. This process took place largely at the end of the Widmanstätten formation, as shown in Figure 1, referring to samples F1 and F2. In F1, the round grains are approximately 18 (±5) µm in diameter and, in F2, the diameters are equal to 35 (±6) µm. By increasing the soaking time (F4 in Figure 1), coarsening caused the austenitic round-shape grains to become islands. After four hours of treatment, the austenitic precipitated, within the ferritic matrix, and disappeared, leaving only the islands present. A negligible amount of small strap-grains was present at the ferritic grain boundaries. In this condition, the ferritic grains were not interrupted by a different phase. After eight hours of treatment (Figure 1, F8), the round austenitic grains appeared

within the ferritic matrix and they were characterised by a diameter equal to 50 (±10) µm, thus bigger than those found in samples F1 and F2. These small grains were a result of the vanishing islands [21,22].

Table 3. Scanning electron microscopy (SEM)-EDS phases chemical composition from Figure 2c.

wt. %	Si	Mo	Cr	Mn	Fe	Ni
Spectrum 0 (α-matrix)	0.90	3.12	23.86	2.01	65.36	4.75
Spectrum 1 (γ-I)	0.62	1.83	22.01	1.41	67.31	6.83
Spectrum 2 (γ-R)	0.54	1.95	21.74	1.23	67.17	7.38
Spectrum 3 (γ-P)	0.52	1.91	21.59	1.42	67.04	7.53
Spectrum 4 (γ-W)	0.56	1.92	21.79	1.44	66.95	7.35
Spectrum 5 (γ-P)	0.53	1.86	21.47	1.27	67.43	7.45

The phase variation is reported in Figure 3, where it is possible to notice that the austenitic quantity did not remain constant during annealing. The austenite fraction decreased from its initial value [18,19], but increased during the soaking, until a peak, which corresponds to 4 h of treatment. At a higher soaking time, the austenite decreased, returning to its previous values.

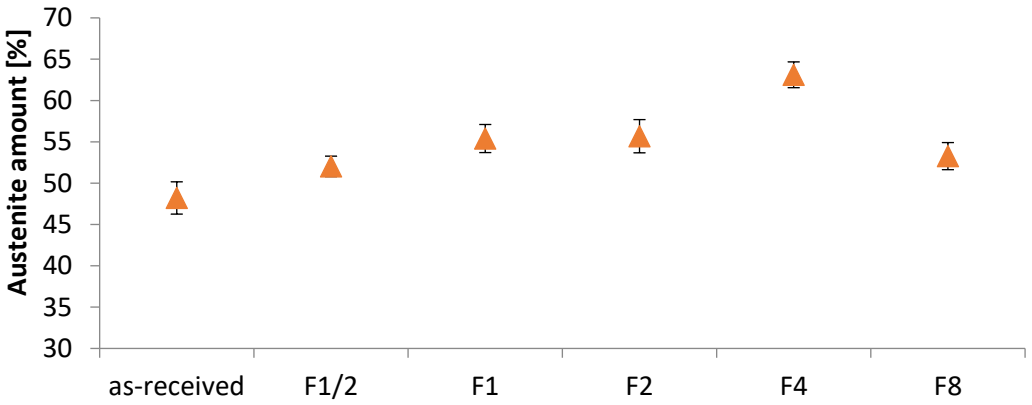

Figure 3. Amount of austenite measured by the ferritoscope.

This trend is the result of the inertia of diffusion and, consequently, the inertia of a changing microstructure. During annealing, diffusion takes place, acting to homogenize the chemical composition and allowing the balance of the phase amount (according to the thermal level) by the nucleation and growth of new grains. In the first annealing period, a diffusion phenomenon was favoured because of the non-homogeneous chemical composition that results from the fast cooling rate of the previous annealing. Even in the early stages of the annealing thermal treatment, the α-matrix experiences a loss of γ-stabilizer elements, which is the driving force for the precipitation processes. Moreover, the fast cooling produces a relevant thermal stress, also associated with the different thermal dilatation of the two phases, which allows the formation of low-energy sites for austenite nucleation [11]. In the first period of the annealing, supported by fast kinetics, the austenite nucleation significantly increased the austenite volume fraction, unbalancing the phase repartitioning. With an increased soaking time, to balance the austenitic fraction, the ferrite began to grow by boundary migration within the austenite.

Figure 4 shows the hardness measurements carried out on each specimen. It is possible to note that the values remain quite constant. The HV was measured in each phase, but only taking into consideration the austenitic islands.

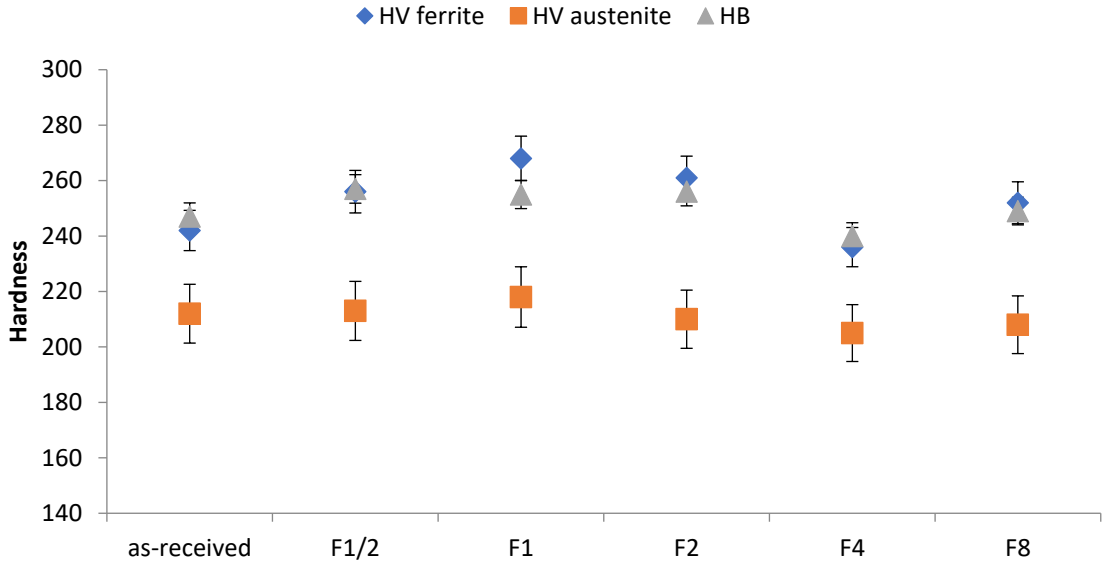

Figure 4. Hardness measurements for different annealing socking times.

The stable hardness trend complies with the material's behaviour and the measurement shows that no precipitation phenomenon has occurred, that is, no hardness modification, confirming that the material was not subjected to a phase change. There was a decrease in ferrite micro-hardness after four hours of treatment. The Brinell numbers confirmed this behaviour. Most probably, this is because of the disappearance of austenitic grains within the ferrite, which led to freely moving dislocations in the crystal, and to lower hardness. Moreover, without austenitic grains, less stress is placed on the ferrite, benefitting the matrix as well.

The ultrasonic attenuation and the related longitudinal sound velocity within the medium are reported in Figure 5.

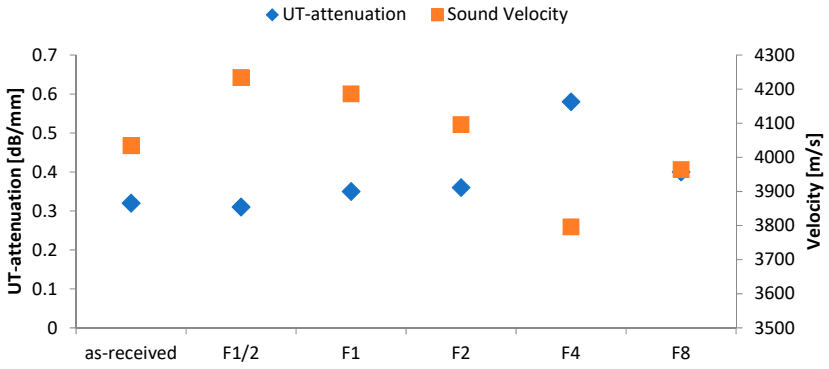

Figure 5. Ultrasonic test (UT)-attenuation results for different annealing socking times.

The attenuation results remain quite constant as the soaking time increases, but exhibit a peak corresponding to F4. After 8 h of treatment, attenuation decreases, but it remains higher than F1 and F2. The velocity reading displays an opposing trend, but features the same behaviour.

All of the samples possessed the same microstructure, composed only by ferrite and austenite, without any types of secondary phases that were able to modify the interaction with sound waves [23]; in this case, the wave propagation was related only to the standard DSS microstructure. Therefore,

the important crystal discontinuities able to affect the propagation were grain boundaries, grain dimensions, and phases distribution.

As mentioned previously, the grain dimension (i.e., the grain boundaries extension) plays an important role in wave scattering. γ-precipitates are grain-nuclei generated during the phase fluctuation to reach the equilibrium amount. These nuclei are smaller than the austenitic island and they tend to vanish as the soaking time increases, allowing the increase of the island itself and a bigger austenitic amount. The attenuation behaviour is related to the scattering owing to these features in relation to the sound's wavelength (Table 4).

Table 4. Influence of austenite precipitates on the scattering regarding the ξ parameter.

Sample	Sound Velocity [m/s]	ξ [μm]	γ-Precipitates [μm]	γ-Precipitates Scattering
as-received	4034	20.17	30	Yes
F1/2	4234	21.17	19	No
F1	4186	20.93	18	No
F2	4096	20.48	35	Yes
F4	3796	18.98	0	No
F8	3964	19.82	50	Yes

The ferritic matrix and the austenitic islands, having a dimension in the order of 100 μm, meet the condition of Rayleigh scattering. On the other hand, the contribution of the γ-precipitates on sound attenuation, caused by grain boundaries scattering, is appreciable in the as-received, F2, and F8 samples, while in the other conditions, it is negligible [3,12].

4. Discussion

The scope of the work was to guarantee the better UT response without negatively affecting the corrosion and mechanical properties of DSS 2205. Therefore, the soaking time was chosen at 1050 °C that guarantees the correct phases and phases ratio. The samples displayed the same structural constituents, ferrite and austenite, as expected for the material and the process performed. The thermal treatments complied varying phase amounts and varying austenite morphology, because of the inertia of reaching the correct phase balance. The different morphologies are the result of their nature (I, W, P, R) and the austenite evolution. This results from the phase amount fluctuating trend around the equilibrium level. It is important to remark that waves propagation is mainly dependent on the material elastic modulus that derives from the nature of the atomic bonds. In all samples, the microstructure is composed by the same phases (sure enough, the hardness test had confirmed no presence of secondary phases); consequently, the elastic modulus remains constant, not leading to any changes in sound attenuation or velocity [18,19,24,25].

During the fluctuation, until reaching the phase balance, the austenite fraction slowly increased before reaching its maximum at F4, which also corresponds to the peak in attenuation. The loss of wave energy owing to the quantity of austenite was confirmed. Indeed, the FCC lattice expended a larger amount of wave energy in order to activate all of the vibrational modes of the cell, which were numerous with respect to the BCC; the attenuation in the austenite is 2.5 times higher than in ferritic steel with a similar grain size [7–9,12,13].

Regarding the ferritic matrix and the austenitic islands, because their dimensions are small in comparison with the wavelength, their scattering contribution on the attenuation is significant [12].

Up to four hours of heating, no changes in attenuation were detected, although the grain morphology underwent significant evolution. Assuming that the Widmanstätten and round-shape grains can be considered as discontinuities in the ferritic matrix, they should have been able to increase the attenuation and decrease the transparency of the material; but they did not. The effect on the wave attenuation is also the result of the relative dimension of the grains with respect to the wavelength of

the beam. As pointed out by ξ in Table 4, the γ-precipitates in sample F1/2 and F1 are small compared with this value, so their contribution to scattering is negligible. Knowing that the scattering condition is "go or go not" [16], they interfere to a lesser extent with the UT-sound, and their contribution to attenuation is only by absorption and diffraction.

In these conditions, the attenuation is mainly owing to the grain nature and not to the presence of γ-discontinuities in the ferritic matrix. It is important to focus on sample F4: it shows the bigger amount of austenite phase with no γ-precipitates; therefore, the austenitic islands must be bigger than in the other cases, allowing a minor ferrite/austenite grain boundaries extension. This should translate into a minor attenuation, which is not the case; thus, the main factor involved in the attenuation is not the scattering owing to the grain boundaries, but to the wave energy loss trying to cross austenite. F2 and F8 samples present a dispersion of big γ-grains within the matrix that are able to attenuate the wave; they react rightly worse then F1/2 and F1, but better then F4 because of a minor amount of austenite island [3,7–9].

When the wave front came across the edge of a reflecting surface, behind this surface, an interference pattern is produced, owing to the phase differences inducing the forward-scattered beam [24]. Despite a grain boundary, or any other interface, reflecting and refracting a sound beam, the wave can continue to propagate as a modified wave, because it must re-form through phase reinforcement and cancellation interference, just to overcome the interface. High beam energy scattering is generated by a large quantity of grain boundaries, hence microstructures with a large quantity of γ-discontinuities promote this kind of dissipation. However, the increase in attenuation owing to such a scattering is lower than that caused by the absorption produced by crystal energy dissipation. Thus, the energy absorption owing to grain boundaries scattering phenomena is less in a matrix free of austenitic discontinuities and the attenuation contribution is mainly caused by the energy dissipation owing to the vibrational modes of the constituent itself, thermal losses, and diffraction [2,7–9,12,13,25,26].

Unfortunately, a comparison, in terms of attenuation, with other alloys is not suitable; duplex stainless steels are a peculiar biphasic material in which one phase results in them being transparent to the UT, while the does other not.

5. Conclusions

The effect of microstructure evolution owing to different annealing times on the attenuation of ultrasonic tests was studied on DSS 2205.

Once the initial attenuation value was measured, the samples underwent different heat treatments featured by different soaking times at 1050 °C. The time was changed in order to promote a microstructural evolution able to influence the UT response.

The following conclusions could be pointed out:

- An increase in the soaking time presents a particular austenite morphology evolution and a fluctuating trend of the phase amount before reaching equilibrium, even so instable;
- The austenitic volume fraction rises, according to this evolution, until a peak that corresponds with a 4 h treatment. After this, the austenite nucleates again within the ferrite;
- The attenuation rears up in correspondence of the major amount of austenite. Then, attenuation decreases again because of the nucleation of new austenitic grains;
- The γ-discontinuities within the ferritic matrix are able to attenuate the wave propagation even by scattering only according to ξ factor;
- The peak in attenuation is detected in the sample showing the highest volume fraction of austenitic island and no γ-discontinuities, which implies that the major effect of attenuation is the grain nature, the related vibrational modes, absorption, and diffraction.

In conclusion, in order to obtain less UT attenuation, without affecting the mechanical and corrosion properties, the soaking should last as little time as possible.

Author Contributions: Conceptualization, S.B., A.G., and C.M.; methodology, A.G.; validation, S.B. and A.G.; investigation, A.G. and D.M.; writing—original draft preparation, A.G.; writing—review and editing, S.B. All authors have read and agreed to the published version of the manuscript.

Funding: This research received no external funding.

Conflicts of Interest: The authors declare no conflict of interest.

References

1. *Le Prove Non Distruttive*, 1st ed.; Associazione Italiana Metallurgia: Milano, Italy, 1999; pp. 245–247.
2. Pandey, D.K.; Pandey, S. Ultrasonics: A Technique of Material Characterization. In *Acoustic Waves*, 1st ed.; Dissanayake D. Intech: Rijeca, Croatia, 2010; pp. 397–430.
3. Nondestructive Evaluation and Quality Control. In *ASM Metals Handbook*, 9th ed.; Ahmad, A.; Bond, L.J. (Eds.) ASM International: Materials Park, OH, USA, 1999; Volume 17.
4. Ahn, B.; Lee, S.S. Effect of microstructure of low carbon steels on ultrasonic attenuation. *IEEE Trans. Ultrason. Ferroelectr. Freq. Control* **2000**, *47*, 620–629. [PubMed]
5. Victoria, B.; George, G.; Kumar, K.A. Ultrasonic Characterization and Micro-Structural Studies On 2205 Duplex Stainless Steel in Thermal Variations. *Int. J. Sci. Tech. Res.* **2015**, *4*, 45–49.
6. Stella, J.; Cerezo, J.; Rodríguez, E. Characterization of the Sensitization Degree in the AISI 304 Stainless Steel Using Spectral Analysis and Conventional Ultrasonic Techniques. *NDT E Int.* **2009**, *4*, 267–274. [CrossRef]
7. Munikoti, V.K. *On the Propagation of Elastic Waves in Acoustically Anisotropic Austenitic Materials and at Their Boundaries during Non-Destructive Inspection with Ultrasound*; Wirtschaftsverl: Berlin, Germany, 2001.
8. Caussin., P.; Cermak, J. Performances of the ultrasonic examination at austenitic steel components. In Proceedings of the Conference on Periodic Inspection of Pressurized Components, London, UK, 8–10 May 1979; p. 207.
9. Edelmann, X. Application of ultrasonic testing techniques on austenitic welds for fabrication and in-service inspection. *NDT Int.* **1981**, *14*, 125–133. [CrossRef]
10. Kittel, C. *Introduction to Solid State Physics*, 8th ed.; John Wiley & Sons: Hoboken, NJ, USA, 2004.
11. Guy, A.G. *Physical Metallurgy for Engineers*, 3rd ed.; Addison Wesley Publishing Company INC: Boston, MA, USA, 1974.
12. Papadakis, E.P. Revised Grain-Scattering Formulas and Tables. *J. Acoust. Soc. Am.* **1965**, *37*, 703. [CrossRef]
13. Bhatia, A.B. *Ultrasonic Absorption*, 1st ed.; Dover Publication: New York, NY, USA, 1985.
14. Ciuffini, A.F.; Barella, S.; Di Cecca, C.; Gruttadauria, A.; Mapelli, C. Microstructural and Phase Ratio Evolution of Superduplex Stainless Steels during Isothermal Annealing at 1080 °C. In Proceedings of the ECHT (European Conference on Heat Treatment) 2015 & 22nd IFHTSE Congress, Venezia, Italy, 20 May 2015.
15. Vander Voort, G.F. Metallography and Microstructure. In *ASM Metals Handbook*; ASM International: Materials Park, OH, USA, 2004; Volume 9.
16. ASTM International. *Standard Guide for Material Selection and Fabrication of Reference Blocks for the Pulsed Longitudinal Wave Ultrasonic Testing of Metal and Metal Alloy Production Material*; E 1158-09; ASTM International: West Conshohocken, PA, USA, 2014.
17. Krautkramer, J.; Krautkramer, H. *Ultrasonic Testing of Materials*, 1st ed.; Springer: Berlin, Germany, 1990.
18. Gunn, R.N. *Duplex Stainless Steels, Microstructure, Properties and Applications*, 1st ed.; Abington Publishing: Cambridge, UK, 1997.
19. Alvarez, I.; Degallaix-Moreuil, A.S. *Duplex Stainless Steels*; Wiley: London, UK, 2009.
20. Nillson, J.O. Super Duplex Stainless Steels. *Mater. Sci. Technol.* **1992**, *8*, 685–700. [CrossRef]
21. Leone, C.L.; Kerr, H.W. The Ferrite to Austenite Transformation in Stainless Steels. *Weld. J.* **1982**, *61*, 13–22.
22. Humphres, F.J.; Hatherly, M. *Recrystallization and Related Annealing Phenomena*, 2nd ed.; Elsevier: Oxford, UK, 2004.
23. Vijayalakshmia, K.; Muthupandib, V.; Jayachitrac, R. Influence of Heat Treatment on the Microstructure, Ultrasonic Attenuation and Hardness of SAF 2205 Duplex Stainless Steel. *Mater. Sci. Eng. A* **2011**, *529*, 447–451. [CrossRef]
24. He, Y.; Zhu, N.; Lu, X.; Li, L. Experimental and Computational Study on Microstructural Evolution in 2205 Duplex Stainless Steel During High Temperature Aging. *Mater. Sci. Eng. A* **2010**, *528*, 721–729. [CrossRef]

25. Barella, S.; Gruttadauria, A.; Mapelli, C.; Mombelli, D.; Fanezi, C.L.; Fioletti, F.; Formentelli, M.; Guarneri, M. Effect of Heat Treatment and of Primary Austenite Grain Size on the Minimum Size of Detectable Defect on 26NiCrMoV11.5 High Strength Steel. *Adv. Eng. Mater.* **2014**, *16*, 103–111. [CrossRef]
26. Ciuffini, A.F.; Barella, S.; Di Cecca, C.; Gruttadauria, A.; Mapelli, C.; Mombelli, D. Isothermal austenite–ferrite phase transformations and microstructural evolution during annealing in super duplex stainless steels. *Metals* **2017**, *7*, 368. [CrossRef]

© 2020 by the authors. Licensee MDPI, Basel, Switzerland. This article is an open access article distributed under the terms and conditions of the Creative Commons Attribution (CC BY) license (http://creativecommons.org/licenses/by/4.0/).